

A model of charmed baryon-nucleon potential and 2- and 3-body bound states with charmed baryon

Saori Maeda^{1,*}, Makoto Oka^{1,2}, Akira Yokota¹, Emiko Hiyama³, and Yan-Rui Liu⁴

¹*Department of Physics, Tokyo Institute of Technology, O-okayama 2-12-1, Meguro, Tokyo 152-8551, Japan*

²*Advanced Science Research Center, Japan Atomic Energy Agency, Tokai, Ibaraki 319-1195, Japan*

³*Nishina Center for Accelerator-Based Science, The institute of Physical and Chemical Research(RIKEN), Wako 351-0198, Japan*

⁴*Department of Physics, Shandong University, Jinan, Shandong 250100, China*

**E-mail: s-maeda@th.phys.titech.ac.jp*

.....

Potential models of the interaction between a charmed baryon (Y_c) and the nucleon (N) are constructed on the basis of a long-range meson (π and σ) exchange potential as well as a short-distance quark exchange interaction. The quark cluster model is used to evaluate the short-range repulsion between Y_c and N , while the meson exchange potentials are modified by a form factor at short distances. We determine the cutoff parameters of the form factors so as to fit the NN scattering data with the same approach. The ground state charmed baryons, Λ_c , Σ_c and Σ_c^* , are included as Y_c , and channel couplings of relevant Y_cN channels are taken into account. We propose four sets of parameters (a – d), among which the most attractive potential (d) predicts bound Λ_cN $J^\pi = 0^+$ and 1^+ states. In order to apply the potential to a many-body problem, we construct an effective Λ_cN one-channel potential for the parameter set (d). It is applied to the 3-body Λ_cNN systems and again spin $1/2$ and $3/2$ bound states are predicted.

.....

Subject Index xxxx, xxx

1. Introduction

Recent development of hadron spectroscopy revealed that there may exist various molecular bound states of hadrons (observed as hadron resonances). In particular, it was indicated to have variety of bound states that include heavy quarks, such as X, Y and Z resonances in the hidden charm/bottom spectrum [1–3]. The quantum chromodynamics (QCD) is flavor independent up to the logarithmic change of the running coupling constant. With the same attractive “potential”, the heavier hadrons are more likely to be bound as the heavy quarks have less kinetic energy.

The above naive expectation motivates us to explore possible bound states of charmed (or bottomed) baryons ($Y_{c(b)}$), *i.e.*, $\Lambda_{c(b)}$, $\Sigma_{c(b)}$ and so on, with the nucleon (N) and/or nucleus. This is, of course, a natural extension of the hypernucleus, which is a nuclear bound state with one or more strange baryons (Y), Λ , Σ , Ξ and so on. Hypernuclear spectroscopy in the last decades was very fruitful in analyzing structures of hypernuclei and extracting information on the YN and YY interactions. Because there is no two-body bound states in ΛN or ΣN systems and it is difficult to perform direct scattering experiments for the hyperons, it is important to get information on their interactions from the three-body or heavier nucleus with strange baryon(s).

The idea of the charmed hypernucleus is, in fact, old [4–10]. It was pointed out [6] that the $SU(4)$ symmetry, though it is badly broken, for the one boson exchange (OBE) models predicts a weaker attraction between Y_c and N , because the K exchange is replaced by the D exchange and it is suppressed by the heavier mass of the D meson. Recent re-analysis with a model based on the heavy quark effective theories has suggested the possibility of bound $Y_c N$ states. There, however, the model has a difficulty of describing the short-range interaction so that its prediction was very sensitive to the cutoff parameters of the one-boson exchange interaction [9].

In this paper, we construct a potential model consisting of the long-range one-pion and one-sigma exchange potential and the quark exchange interaction based on the quark cluster model of the baryon-baryon interaction [11, 12]. The latter provides a short range repulsion between Y_c and N . Adjusting the meson exchange parameters to reproduce low-energy data of the NN system, we propose four sets of the $Y_c N$ potential. Here Y_c represents Λ_c , Σ_c and Σ_c^* , and the potential contains the off-diagonal components, which couple $\Lambda_c N$, $\Sigma_c N$ and $\Sigma_c^* N$ channels of the same total quantum numbers.

We solve the coupled channel Schrödinger equation using the Gaussian expansion method (GEM) [13] and obtain $\Lambda_c N$ bound states. The potential is also applied to the three-body system, $\Lambda_c NN$, and bound states and their properties are analyzed.

The paper is organized as follows. In Sect. 2, we present our model of the $Y_c N$ potential and explain how the model parameters are determined. In Sect. 3, the two-body $Y_c N$ systems are analyzed for the given potentials and the results are examined. In Sect. 4, we construct an effective one-channel $\Lambda_c N$ potential model and apply it to the three-body $\Lambda_c NN$ system. Conclusions are given in Sect. 5.

2. Model of $Y_c N$ interactions

We first consider the two-baryon systems, $Y_c N$, with isospin $I = \frac{1}{2}$ and spin-parity $J^\pi = 0^+$ or 1^+ . Table 1 gives possible channels given by $\Lambda_c N$, $\Sigma_c N$, and $\Sigma_c^* N$ for each J . The channels

Channels	1	2	3	4	5	6	7
$J^\pi = 0^+$	$\Lambda_c N(^1S_0)$	$\Sigma_c N(^1S_0)$	$\Sigma_c^* N(^3D_0)$				
$J^\pi = 1^+$	$\Lambda_c N(^3S_1)$	$\Sigma_c N(^3S_1)$	$\Sigma_c^* N(^3S_1)$	$\Lambda_c N(^3D_1)$	$\Sigma_c N(^3D_1)$	$\Sigma_c^* N(^3D_1)$	$\Sigma_c^* N(^5D_1)$

Table 1 The S-wave $\Lambda_c N$ states and the channels which couple to them [9]

with the orbital angular momentum $L = 0$ and 2 will be coupled by tensor potentials, while those with same L are coupled mainly by central potentials. We solve coupled channel Shorödinger equation for a hybrid potential model. The model consists of exchanges of a pion and a scalar σ meson for long-range interactions [9] and a short-range repulsive potential coming from the quark exchanges between the baryons [11].

2.1. One boson exchange potential

The meson exchange parts contain the spin-independent central, spin-spin, tensor and the spin-orbit potentials,

$$\begin{aligned}
V_\pi(i, j) &= C_\pi(i, j) \frac{m_\pi^3}{24\pi f_\pi^2} \left\{ \langle \mathcal{O}_{spin} \rangle_{ij} Y_1(m_\pi, \Lambda_\pi, r) + \langle \mathcal{O}_{ten} \rangle_{ij} H_3(m_\pi, \Lambda_\pi, r) \right\} \\
V_\sigma(i, j) &= C_\sigma(i, j) \frac{m_\sigma}{16\pi} \left\{ \langle \mathbf{1} \rangle_{ij} 4Y_1(m_\sigma, \Lambda_\sigma, r) + \langle \mathcal{O}_{LS} \rangle_{ij} \left(\frac{m_\sigma}{M_N} \right)^2 Z_3(m_\sigma, \Lambda_\sigma, r) \right\}
\end{aligned} \tag{1}$$

where i and j are the labels of the channels and $C_\pi(i, j)$ and $C_\sigma(i, j)$ are the relevant coupling constants including the isospin factor. The spin dependent operators, \mathcal{O}_{spin} , \mathcal{O}_{ten} , and \mathcal{O}_{LS} , and their expectation values are given in Appendix A. The r -dependent functions, Y_1 , H_3 , and Z_3 , contain the cutoff parameters, Λ_π , Λ_σ and their explicit forms are given in Appendix B. The coupling strength and the cutoff parameters are determined later.

2.2. Short range repulsion from Quark Cluster Model

In a previous approach [9], we considered exchanges of the vector mesons for short range part of the $Y_c N$ interaction. They, however, do not provide enough repulsion at short distances and result in very deep bound states with compact wave functions. As the wave function of the baryons overlap significantly at short distances, we here consider quark exchange interactions of the quark cluster model(QCM) [11].

The QCM consider clusters each made of three quarks as baryons. When two clusters overlap at small r , the quark exchanges are induced by the antisymmetrization among the (light) quarks and thus give a non-local interaction. When two baryons overlap completely i.e., $r = 0$, all the six quarks occupy the lowest energy orbit with a single center. Such states are approximately given by a product of the Gaussian wave functions with an appropriate symmetry accordingly to the quantum numbers. The strengths of the repulsive potential at $r = 0$ are thus given by the difference of the expectation values of the quark model Hamiltonian for the single-centered six-quark states and for the individual baryons.

$$V_0 \approx \langle 6q | H | 6q \rangle - 2 \langle 3q | H | 3q \rangle \tag{2}$$

It happens [11] that the strengths are sensitive to and determined dominantly by the color-magnetic interaction (CMI) given by

$$V_{CM} = -\beta \sum_{i < j} (\boldsymbol{\sigma}_i \cdot \boldsymbol{\sigma}_j)(\boldsymbol{\lambda}_i \cdot \boldsymbol{\lambda}_j) \quad (3)$$

where $\boldsymbol{\sigma}_i$ and $\boldsymbol{\lambda}_i$ are the spin and color operators of the i -th quark. The expectation values of the color-magnetic operator for a five light quark systems can be computed by using the formula,

$$\langle V_{CM} \rangle = \beta \left[8N + \frac{4}{3}S(S+1) + 2C_2[SU(3)_c] - 4C_2[SU(6)_{cs}] \right], \quad (4)$$

where N is the numbers of light quarks included in baryons, S is the total spin, and $C_2[SU(g)]$ is the quadratic Casimir operator, given for the representation specified by the Young diagram $[f_1, \dots, f_g]$ as

$$C_2[SU(g)] = \frac{1}{2} \left[\sum_i f_i(f_i - 2i + g + 1) - \frac{N^2}{g} \right]. \quad (5)$$

The overall strength β can be determined by the $\Delta(1232)$ - nucleon (N) mass splitting, which comes also from V_{CM} . From $\langle V_{CM} \rangle_{\Delta} - \langle V_{CM} \rangle_N = -16\beta = 293\text{MeV}(\text{exp.})$, we obtain $\beta \cong 18.2$ MeV. Table 2 shows the values of V_{CM} for various two-baryon (six-quark) states. These values correspond to the heavy quark limit, so that the heavy quark spin does not contribute.

System	V_0 [MeV]
$(NN)_{I=1}^{S=0}$	450
$(NN)_{I=0}^{S=1}$	350
$(\Lambda_c N)_{I=1/2}^{S=0}$	300
$(\Lambda_c N)_{I=1/2}^{S=1}$	300

$$\begin{pmatrix} \Sigma_c N \\ \Sigma_c^* N \end{pmatrix}_{I=1/2}^{S=0} = \begin{pmatrix} 100 & 0 \\ 0 & 0 \end{pmatrix} \quad \begin{pmatrix} \Sigma_c N \\ \Sigma_c^* N \end{pmatrix}_{I=1/2}^{S=1} = \begin{pmatrix} 166.7 & -24.0 \\ -24.0 & 108.3 \end{pmatrix}$$

Table 2 Expectation values of the color magnetic interaction (CMI) for the relevant channels. We assume the heavy quark limit. For the channel couplings of $\Sigma_c N$ and $\Sigma_c^* N$, the values are shown in the matrix form.

We assume, for simplicity, that the radial dependence of the QCM potential is given by a Gaussian,

$$V_{QCM} = V_0 e^{-(r^2/b^2)}. \quad (6)$$

The range parameter b is supposed to coincide with the extension of the quark wave functions in the baryon. According to [12], the typical values for the NN interaction are about $0.54 \sim 0.58$ fm. For the $Y_c N$ systems, we use two typical values, $b = 0.5$ and 0.6 fm, and compute the results.

2.3. Coulomb potential

We also include the Coulomb potential between the charged baryons. In this calculation, we consider only the two-baryon channels which couple to $\Lambda_c N (I = \frac{1}{2})$. For the $\Lambda_c n$ system (total charge $Q = +1$), we have no Coulomb effect. For the $Q = 2$ channels, $\Lambda_c p$, $\Sigma_c^+ p$ and $\Sigma_c^{++} n$, we assume that the mixing of $\Sigma_c^+ p$ and $\Sigma_c^{++} n$ is not modified by the Coulomb interaction and approximate the Coulomb potential for the $I = \frac{1}{2}$ combination,

$$\left| (\Sigma_c N)_{I=\frac{1}{2}, I_3=+\frac{1}{2}} \right\rangle = -\sqrt{\frac{1}{3}} \left| \Sigma_c^+ p \right\rangle + \sqrt{\frac{2}{3}} \left| \Sigma_c^{++} n \right\rangle \quad (7)$$

Then the "effective" Coulomb potentials for the $Y_c N$ channels are given by

$$\begin{aligned} V_{coulomb}^{\Lambda_c N}(r) &= \frac{\alpha \hbar c}{r}, \\ V_{coulomb}^{\Sigma_c N}(r) &= \frac{1}{3} \frac{\alpha \hbar c}{r}, \\ V_{coulomb}^{\Sigma_c^* N}(r) &= \frac{1}{3} \frac{\alpha \hbar c}{r}, \end{aligned} \quad (8)$$

where $\alpha = 1/137$ is the fine structure constant.

2.4. Determining the potential parameters

In the previous study using the OBE potential [9], we found that the results are very sensitive to the cutoff parameters, Λ . To remedy this problem, in the present approach, we determine the parameters of the potential so as to reproduce the NN interaction data using the same model. In doing so, we fix the π -baryon coupling constants and the short-range parts derived from the quark model. Then the cutoffs, Λ_π and Λ_σ , and the sigma coupling constant, C_σ , are the parameters to be determined in the NN system. Then the results are generalized to the $Y_c N$ system, assuming that the light mesons couple only to the light quarks, and the cutoff parameters are common to NN and $Y_c N$ systems. The details are given in Appendix B. We use the deuteron binding energy for the $J^\pi = 1^+$ potential and the $NN(^1S_0)$ scattering length for the 0^+ potential.

In solving the Schrödinger equation for the two-baryon system, we employ a variational method with Gaussian trial functions, the Gaussian Expansion Method [13], where the radial wave functions are expanded by the basis states given by Gaussian functions with varied range parameters.

$$\begin{aligned} \psi_{lm}(\mathbf{r}) &= \sum_{n=1}^{n_{max}} c_{nl} \phi_{nlm}^G(\mathbf{r}) \\ \phi_{nlm}^G(\mathbf{r}) &= \phi_{nl}^G(r) Y_{lm}(\hat{\mathbf{r}}) \\ \phi_{nl}^G(r) &= N_{nl} r^l e^{-\nu_n r^2} \\ \nu_n &= \frac{1}{r_n} = \frac{1}{r_1 a^{n-1}} \end{aligned} \quad (9)$$

This method has been applied to various bound state problems and is proved to give an accurate approximation to the eigen-energies and wave functions.

In searching the three undetermined parameters, Λ_π , Λ_σ and C_σ , we use the following experimental values of the NN interaction,

$$\begin{aligned} NN(^1S_0) \text{ scattering length} &= -23.7 \text{ fm}, \\ NN(^3S_1) \text{ binding energy (deuteron)} &= 2.22 \text{ MeV}. \end{aligned} \quad (10)$$

We set the possible range of the parameters to search appropriate values as

$$\begin{aligned}\Lambda_\pi &= 500 \sim 900 \text{ MeV}, \\ \Lambda_\sigma &= 900 \sim 1200 \text{ MeV}, \\ C_\sigma(NN) &= -64.0 \sim -225.0.\end{aligned}\tag{11}$$

and searched the solution, but we could not find one. Therefore we relax a condition that C_σ is independent of J^π and take $C_\sigma(J^\pi = 0^+)$ and $C_\sigma(J^\pi = 1^+)$ independently. Then we find solutions, given in Tables 3 and 4, of the values of the parameters ($\Lambda_\pi, \Lambda_\sigma, C_\sigma(J^\pi = 0^+)$ and $C_\sigma(J^\pi = 1^+)$) determined for $b = 0.6$ fm and $b = 0.5$ fm, respectively. In Table 3, we fix $\Lambda_\pi = 750$ MeV and Λ_σ is varied, while, on the other hand, Table 4 shows the results with varied Λ_π for a fixed $\Lambda_\sigma = 1000$ MeV. Tables 3 and 4 also give the differences of $C_\sigma(J^\pi = 0^+)$ and $C_\sigma(J^\pi = 1^+)$,

$$\Delta_C = |C_\sigma(J^\pi = 0^+) - C_\sigma(J^\pi = 1^+)|.\tag{12}$$

We suppose that the spin dependence of C_σ is small, so that a small Δ_C is favored. Tables 3 and 4 show that Δ_C is insensitive to the change of Λ_σ , but Δ_C increases rapidly for increasing Λ_π . The results for $b = 0.5$ fm and 0.6 fm are qualitatively similar. Since the QCM repulsion is weaker than that for $b = 0.6$ fm, the resulting C_σ is also smaller and Δ_C tends to be smaller for $b = 0.5$ fm.

	$b = 0.6[\text{fm}]$			$b = 0.5[\text{fm}]$		
$\Lambda_\sigma[\text{MeV}]$	$C_\sigma(0^+)$	$C_\sigma(1^+)$	Δ_C	$C_\sigma(0^+)$	$C_\sigma(1^+)$	Δ_C
900	-213.16	-161.29	51.87	-176.89	-132.25	44.64
950	-179.56	-134.56	45.0	-148.84	-110.25	38.59
1000	-156.25	-118.81	37.44	-129.96	-96.04	33.92
1050	-141.61	-106.09	35.52	-116.64	-86.49	30.15
1100	-127.69	-96.04	31.65	-106.09	-79.21	26.88
1150	-116.64	-88.36	28.28	-98.01	-72.25	25.76
1200	-108.16	-82.81	25.35	-90.25	-67.24	23.01

Table 3 The NN 2-body parameters for $\Lambda_\pi = 750$ MeV

The resulting NN potentials for $J^\pi = 0^+$ with various obtained parameters are plotted in Figs. 1 and 2. We find that some of the potentials (for small Λ_π) are strongly attractive at short distances and may not be appropriate for the current purposes, although they all reproduce the 1S_0 scattering length or the deuteron binding energy.

Therefore we choose $\Lambda_\pi = 750$ MeV and $\Lambda_\sigma = 1000$ MeV and we find four sets of the most realistic potential parameters, given in Table 5. We call these models “ Y_cN -CTNN” potentials, as these parameter sets correspond to the NN experimental data.

3. Y_cN bound states

The Y_cN potentials derived for $J^\pi = 0^+$ are shown in Figs. 3 - 8. Components of the Y_cn CTNN-a potential and the Y_cN potentials derived for $J^\pi = 1^+$ are given in Appendix C. Since V_π is fixed with these parameter, non-diagonal parts affected to large tensor force

	$b = 0.6[\text{fm}]$			$b = 0.5[\text{fm}]$		
$\Lambda_\pi[\text{MeV}]$	$C_\sigma(0^+)$	$C_\sigma(1^+)$	Δ_C	$C_\sigma(0^+)$	$C_\sigma(1^+)$	Δ_C
500	-148.84	-139.24	9.6	-118.81	-121.0	2.19
550	-151.29	-136.89	14.4	-123.21	-116.64	6.57
600	-153.76	-134.56	19.2	-125.44	-114.49	10.95
650	-153.76	-129.96	23.8	-127.69	-110.25	17.44
700	-156.25	-125.44	30.81	-127.69	-104.04	23.65
750	-156.25	-118.81	37.44	-129.96	-96.04	33.92
800	-156.25	-110.25	48.51	-129.96	-88.36	41.6
850	-156.25	-102.01	54.24	-132.25	-79.21	53.04
900	-156.25	-92.16	66.6	-132.25	-70.56	61.69

Table 4 The NN 2-body parameters for $\Lambda_\sigma = 1000$ MeV

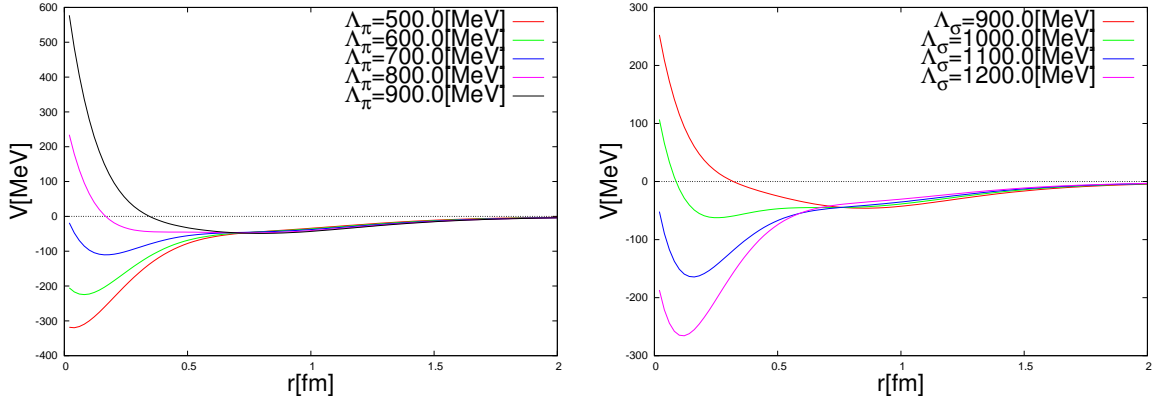


Fig. 1 NN potential ($J^\pi = 0^+$) for $b=0.6\text{fm}$ and $\Lambda_\sigma = 1000$ MeV. **Fig. 2** NN potential ($J^\pi = 0^+$) for $b=0.6\text{fm}$ and $\Lambda_\pi = 750$ MeV.

	C_σ	$b[\text{fm}]$
parameter a	-67.58	0.6
parameter b	-77.5	0.6
parameter c	-60.76	0.5
parameter d	-70.68	0.5

Table 5 The CTNN potential parameters

in channel couplings have same potential. On the other hand, V_σ and QCM repulsion are predominant in diagonal parts, and total potential is different for each parameter.

For $Y_c p$ potential, we add the Coulomb potential to the potentials as eq. (8). Effects of the Coulomb repulsion is very weak and concentrated mostly in the short-range part of about 0.5 fm.

The $Y_c N$ binding energies are given in Tables 6 and 7. The $\Lambda_c n$ systems ($J^\pi = 0^+$ or 1^+) without the Coulomb potential have a bound state for the $Y_c N$ -CTNN parameter b, c, and d. The CTNN-b and c potential has a very shallow bound state and the CTNN-d potential

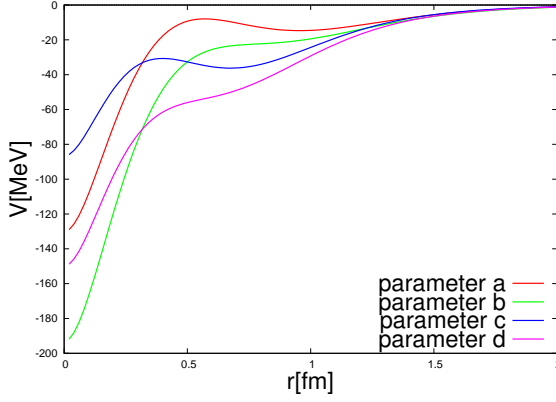


Fig. 3 Y_cN -CTNN potential for the $\Lambda_c N$ single channel.

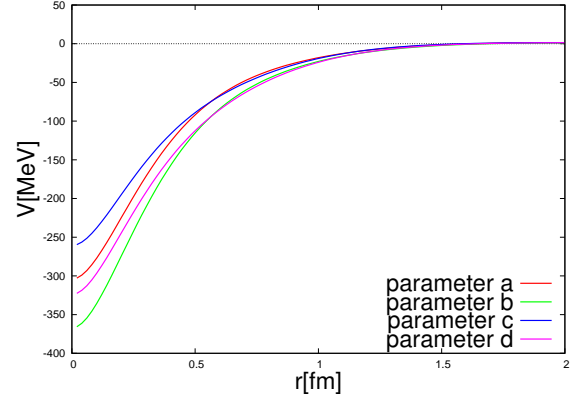


Fig. 4 Y_cN -CTNN potential for the $\Sigma_c N$ single channel.

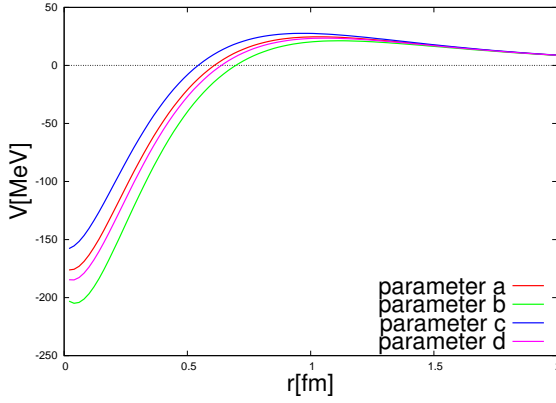


Fig. 5 Y_cN -CTNN potential for the $\Sigma_c^* N$ single channel.

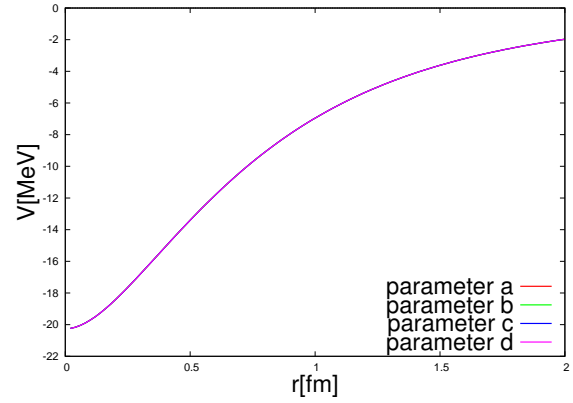


Fig. 6 Y_cN -CTNN potential for the $\Lambda_c N$ - $\Sigma_c N$ channels.

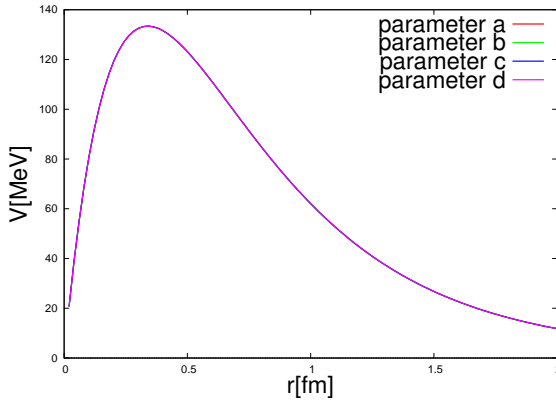


Fig. 7 Y_cN -CTNN potential for the $\Lambda_c N$ - $\Sigma_c^* N$ channels.

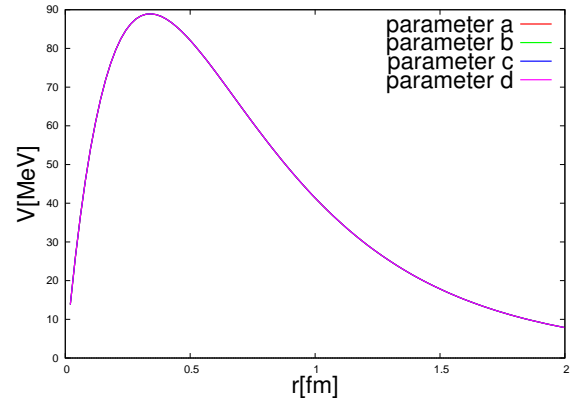


Fig. 8 Y_cN -CTNN potential for the $\Sigma_c N$ - $\Sigma_c^* N$ channels.

gives a larger binding energy. The CTNN-a and -b have stronger QCM repulsion at short distances, so it indicates that the effect of the repulsion is significant. On the other hand, $\Lambda_c p$ with the Coulomb potential has a bound state only for the parameter CTNN-d.

$J^\pi = 0^+$	CTNN-a	CTNN-b	CTNN-c	CTNN-d
B.E. [MeV]	-	-	1.72×10^{-3}	1.37
(+ Coulomb)				(0.56)
scattering length [fm]	-3.64	-65.15	130.93	5.31
probability($\Lambda_c N$)[%]	-	-	99.97	99.29
probability($\Sigma_c N$)[%]	-	-	7.0×10^{-3}	0.20
probability($\Sigma_c^* N$)[%]	-	-	2.1×10^{-2}	0.51

Table 6 Binding energies of $\Lambda_c N$ ($J^\pi = 0^+$) for the CTNN potentials. The probabilities of the $\Sigma_c N$ and $\Sigma_c^* N$ channels are also shown.

$J^\pi = 1^+$	CTNN-a	CTNN-b	CTNN-c	CTNN-d
B.E. [MeV]	-	1.67×10^{-4}	1.91×10^{-2}	1.56
(+ Coulomb)				(0.72)
scattering length [fm]	-4.11	337.53	39.27	5.01
probability($\Lambda_c N$)[%]	-	99.99	99.90	99.23
probability($\Sigma_c N$)[%]	-	4.9×10^{-3}	4.9×10^{-2}	0.39
(D-wave (3D_1))	-	4.5×10^{-3}	4.6×10^{-2}	0.35
probability($\Sigma_c^* N$)[%]	-	4.6×10^{-3}	4.6×10^{-2}	0.38
(D-wave (5D_1))	-	3.1×10^{-3}	3.2×10^{-2}	0.25

Table 7 Binding energies of $\Lambda_c N$ ($J^\pi = 1^+$) for the CTNN potentials. The probabilities of the coupled D-wave $\Lambda_c N$ and $\Sigma_c N$ and $\Sigma_c^* N$ channels are also shown.

The $\Lambda_c N$ scattering lengths for the CTNN potentials are given in Tables 6 and 7. These results are consistent with the binding energies.

The above results show that binding energies of the $J^\pi = 1^+$ bound states are larger than those of $J^\pi = 0^+$. Our results are consistent with the previous study [9], so that the bound solutions with small cutoff parameters have small binding energies.

Table 7 also shows the probabilities of the coupled channels. In all the parameter sets and the total angular momenta, the probability of $\Lambda_c N$ is more than 99 %. In $J^\pi = 0^+$, the probability of $\Sigma_c^* N$ (5D_0) is larger than that of $\Sigma_c N$ (1S_0). On the other hand, in $J^\pi = 1^+$, the respective total probabilities of $\Sigma_c N$ and $\Sigma_c^* N$ are almost equal. Looking closely, $\Sigma_c N$ (3S_1) and $\Sigma_c^* N$ (5D_1) contribute largely to the results. These results are explained by the contributions of the strong tensor force between the $\Lambda_c N$ ($L = 0$) and $\Sigma_c N$ / $\Sigma_c^* N$ ($L = 2$) states.

4. $\Lambda_c NN$ systems

4.1. Effects of channel couplings

In the previous section, we find that the probabilities of the $\Lambda_c N$ component are almost 100% and the mixings of $\Sigma_c N$ or $\Sigma_c^* N$ are small. However, effects of the $\Sigma_c N - \Sigma_c^* N$ channel couplings are important for binding the $\Lambda_c N$ system, because the single channel calculations of $\Lambda_c N$ do not have a bound state for all the CTNN-a \sim d potentials.

	$\Lambda_c N - \Sigma_c N - \Sigma_c^* N$		$\Lambda_c N$		$\Lambda_c N - \Sigma_c N$		$\Lambda_c N - \Sigma_c^* N$	
J^π	0^+	1^+	0^+	1^+	0^+	1^+	0^+	1^+
CTNN-a	-3.63	-4.10	-1.11	-1.11	-1.16	-2.07	-3.13	-2.09
CTNN-b	-63.25	398.67	-2.62	-2.62	-2.78	-6.74	-20.84	-7.00
CTNN-c	139.07	39.96	-3.01	-3.01	-3.19	-8.61	-48.56	-9.00
CTNN-d	5.32	5.02	-28.59	-28.59	-44.65	9.79	6.01	9.36
B.E.	1.37	1.56	-	-	-	0.36	1.04	0.39

Table 8 Scattering lengths in fm, and the two-body binding energies in MeV for the cases when the number of the coupled channels is reduced to $\Lambda_c N$ only, $\Lambda_c N - \Sigma_c N$ or $\Lambda_c N - \Sigma_c^* N$

In Table 8, we show the scattering lengths obtained for partially coupled systems, i.e., the single $\Lambda_c N$, $\Lambda_c N - \Sigma_c N$, and $\Lambda_c N - \Sigma_c^* N$ coupled-channel systems. It is found that only the CTNN-d potential has bound states in the $\Lambda_c N - \Sigma_c^* N$ (0^+ and 1^+) and the $\Lambda_c N - \Sigma_c N$ (1^+) systems. In particular, effect of the $\Sigma_c^* N$ (0^+) channel is large so that without $\Sigma_c^* N$ (5D_0) no bound state is found. This indicates that the tensor force from the one-pion exchange, which induces the coupling of $\Sigma_c^* N$ (5D_0) and $\Lambda_c N$ (1S_0), is significant. Similarly, the contributions of the tensor force and $\Sigma_c N - \Sigma_c^* N$ couplings are found to be important for the $J^\pi = 1^+$ state.

4.2. Effective $\Lambda_c N$ potential

In order to apply the obtained potentials to many-body systems with Λ_c , we construct single-channel $\Lambda_c N$ potentials, in which the effects of the $\Sigma_c N - \Sigma_c^* N$ couplings are effectively taken into account. We assume two-range Gaussian forms,

$$\begin{aligned}
V_{\text{eff}}^{0+} &= V_1^{0+} e^{-\frac{r^2}{b_1^2}} + V_2^{0+} e^{-\frac{r^2}{b_2^2}}, \\
V_{\text{eff}}^{1+} &= V_1^{1+} e^{-\frac{r^2}{b_1^2}} + V_2^{1+} e^{-\frac{r^2}{b_2^2}}.
\end{aligned} \tag{13}$$

Here, b_1 and b_2 are range parameters, and V_1^{JP} and V_2^{JP} are the strength parameters. These parameters are determined from the CTNN potentials described as follows. For simplicity, we choose the same b_1 and b_2 for $J^\pi = 0^+$ and 1^+ , and rewrite eq. (13) to

$$V_{\text{eff}_{Y_{cN}}} = [V_r^1 + \boldsymbol{\sigma}_{\Lambda_c} \cdot \boldsymbol{\sigma} V_s^1] e^{-\frac{r^2}{b_1^2}} + [V_r^2 + \boldsymbol{\sigma}_{\Lambda_c} \cdot \boldsymbol{\sigma} V_s^2] e^{-\frac{r^2}{b_2^2}}, \tag{14}$$

$$\begin{aligned}
V_r^i &= \frac{1}{4}(V_i^{0+} + 3V_i^{1+}), \\
V_s^i &= \frac{1}{4}(V_i^{1+} - V_i^{0+}).
\end{aligned} \tag{15}$$

Now, we consider only the Y_{cN} -CTNN-d potential to construct an effective potential which reproduces the binding energy and scattering length of the channel coupling calculations in $J^\pi = 0^+$ and 1^+ . We search the parameters, assuming that the first term, V_1 of eq. (13) is an attractive potential like OBEP and the second term, V_2 is repulsive like the QCM repulsion. We choose b_1 and b_2 accordingly, namely b_2 is taken from the radius of the quark wave function, $b_2 = 0.5\text{fm}$. On the other hand, b_1 is chosen to represent a typical range of the meson exchange potential which couples $\Lambda_c N$ to $\Sigma_c N$ and $\Sigma_c^* N$, $b_1 = 0.9\text{fm}$.

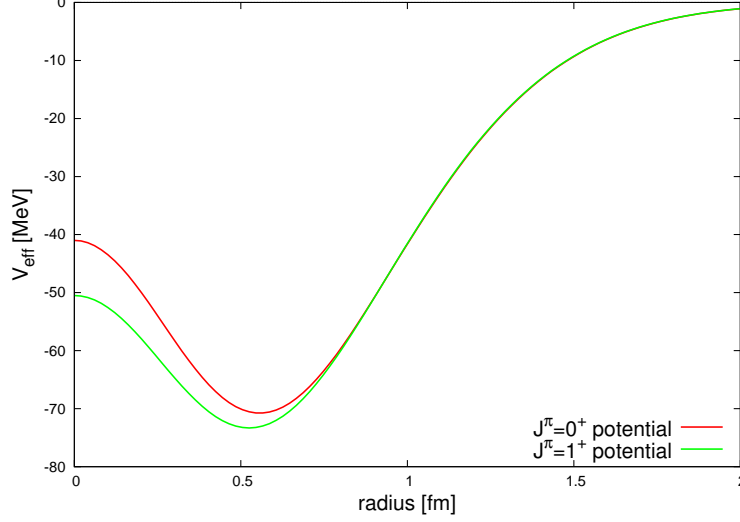


Fig. 9 $\Lambda_c N$ effective potentials for $J^\pi = 0^+$ and 1^+ .

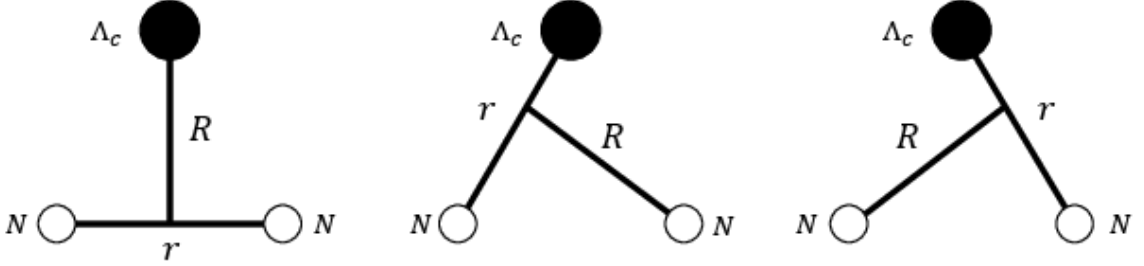


Fig. 10 Jacobi coordinates for $\Lambda_c NN$.

The parameters of the effective potential are chosen as

$$V_1^{0+} = -150.0[\text{MeV}], \quad V_2^{0+} = 109.0[\text{MeV}], \quad V_1^{1+} = -149.0[\text{MeV}], \quad V_2^{1+} = 98.5[\text{MeV}]. \quad (16)$$

Fig. 9 shows the shape of the effective potentials.

The effective potential can be expressed in the strengths of the spin-independent, V_r , and the spin-spin, V_s , terms, defined by eq. (14) as

$$V_r^1 = -149.25[\text{MeV}], \quad V_s^1 = 0.25[\text{MeV}], \quad V_r^2 = 101.125[\text{MeV}], \quad V_s^2 = -2.625[\text{MeV}]. \quad (17)$$

One sees that the spin dependent potential is weak. This is a consequence of the heavy quark spin symmetry [19–22].

4.3. $\Lambda_c NN$ bound states

Next, we consider the calculation of $\Lambda_c NN$ three-body system using the $\Lambda_c N$ effective potential given in the previous section.

In this calculation, we adopt to Jacobi coordinates shown in Fig. 10. The angular momenta, l and L are defined corresponding to r and R , respectively. On the other hand, the spin assignments are defined for two nucleons, S_{NN} , and total spin, S_{tot} . For $I = 0$, the binding energy is calculated from the threshold of Λ_c plus the deuteron, while for $I = 1$, the threshold is the bound state of $\Lambda_c N$ ($B=1.56$ MeV) plus a nucleon.

In this calculation, we assume that the angular momenta l and L are zero only. Then S_{NN} and I are related and possible J^π are given for each I as

$$\begin{aligned} I = 0 & \quad \cdots \quad S_{NN} = 1, \text{ and } J^\pi = \frac{1}{2}^- \text{ and } \frac{3}{2}^-, \\ I = 1 & \quad \cdots \quad S_{NN} = 0, \text{ and } J^\pi = \frac{1}{2}^-. \end{aligned} \quad (18)$$

From various potential models of NN system [14–18], we employ the Minnesota potential [14]. It describes the deuteron only with S-wave component, as the contribution D-wave mixing is effectively taken into account in the central potential,

$$V_{ij}(r) = \left(V_R + \frac{1}{2}(1 + P_{ij}^\sigma)V_t + \frac{1}{2}(1 - P_{ij}^\sigma)V_s \right) \left(\frac{1}{2}u + \frac{1}{2}(2 - u)P_{ij}^r \right) \quad (19)$$

$$V_R(r) = V_{0R}e^{-\kappa_R r^2}, \quad V_t(r) = V_{0t}e^{-\kappa_t r^2}, \quad V_s(r) = V_{0s}e^{-\kappa_s r^2} \quad (20)$$

$$\begin{aligned} V_{0R} &= 200.0[\text{MeV}], \quad \kappa_R = 1.487[\text{fm}^{-2}], \\ V_{0t} &= -178.0[\text{MeV}], \quad \kappa_t = 0.639[\text{fm}^{-2}], \\ V_{0s} &= -91.85[\text{MeV}], \quad \kappa_s = 0.465[\text{fm}^{-2}]. \end{aligned} \quad (21)$$

We use GEM [13] to the three-body system as with the two-body system. The binding energies of the $\Lambda_c NN$ three-body system with $\Lambda_c N$ effective potential are shown in Fig. 11. The left two plots in Fig. 11 show the results for $I = 0$ without and with Coulomb potential, respectively. The others represent the results of $\Lambda_c nn$, $\Lambda_c np$, $\Lambda_c pp$ for $I = 1$. For all the systems, we find a bound state. Because the spin-spin interaction between Λ_c and N is weak as is seen in Table 7, the binding energies of $J^\pi = \frac{1}{2}^+$ and $\frac{3}{2}^+$ are close to each other in $I = 0$. These results agree well with the heavy quark spin symmetry [19]. In the present calculation, we find that the $\frac{3}{2}^+$ state is lower in energy than the $\frac{1}{2}^+$ state by about 0.7 MeV. These results are consistent with a recent three-body calculation [10], which also found the $\frac{3}{2}^+$ $\Lambda_c NN$ as the lowest state. Effect of the Coulomb potential between Λ_c and proton is smaller than the difference between the $I = 0$ and 1 results.

	Binding energy [MeV] (From threshold)		r [fm]	R [fm]
$\Lambda_c np$ w/o Coulomb $J^\pi = \frac{1}{2}^+$	21.78	19.56	1.91	1.34
$\Lambda_c np$ w/o Coulomb $J^\pi = \frac{3}{2}^+$	22.46	20.24	1.90	1.32
$\Lambda_c np$ w/ Coulomb $J^\pi = \frac{1}{2}^+$	20.43	18.21	1.93	1.36
$\Lambda_c np$ w/ Coulomb $J^\pi = \frac{3}{2}^+$	21.09	18.87	1.91	1.34

Table 9 $\Lambda_c NN$ binding energies and particle distances for the $I = 0$ bound states

Tables 9 and 10 show the mean distances in the bound state, where r is the root mean square (rms) distance between the nucleons, and R is rms distance between Λ_c and the center

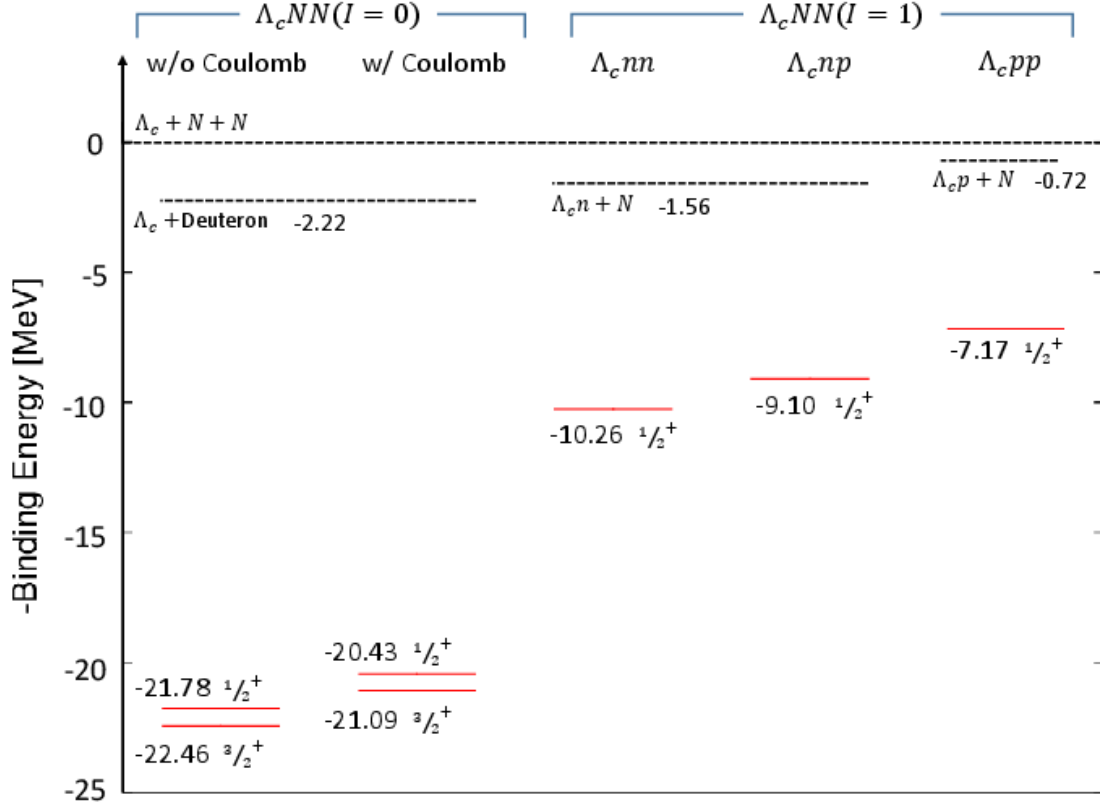


Fig. 11 $\Lambda_c NN$ binding energies. The dotted lines show the Λ_c -deuteron threshold that is 2.22 MeV below the $\Lambda_c NN$ threshold, the threshold of the $(\Lambda_c n)$ 1^+ bound state plus a nucleon, i.e., 1.56 MeV below $\Lambda_c NN$, and the threshold of the $(\Lambda_c p)$ 1^+ bound state plus a nucleon, i.e., 0.72 MeV below $\Lambda_c NN$

	Binding energy [MeV]	(From threshold)	r [fm]	R [fm]
$\Lambda_c nn$ $J^\pi = \frac{1}{2}^+$	10.26	8.70	2.62	1.64
$\Lambda_c np$ $J^\pi = \frac{1}{2}^+$	9.10	7.54	2.67	1.68
$\Lambda_c pp$ $J^\pi = \frac{1}{2}^+$	7.17	6.35	2.78	1.75

Table 10 $\Lambda_c NN$ binding energies and particle distances for the $I = 1$ bound states

of mass of NN . These tables show that the mean NN separations, r , are significantly smaller than the mean distance of $p - n$ in the deuteron, about 3.8 fm. Namely, the Λ_c attraction to the nucleon makes the $\Lambda_c NN$ system shrink. It is also seen that R is smaller than r . Thus we can draw an intuitive picture that the nucleons go around Λ_c sitting at the center in the $\Lambda_c NN$ system. This property is also seen in the hypernuclei system, but the attractive force in the charmed nuclei system is stronger than that in the hypernuclei system.

5. Conclusion

We have examined the interactions between the ground-state charmed baryons, Λ_c , Σ_c and Σ_c^* , and the nucleon, N . A potential model is proposed, composed of the long-range one-boson exchange (OBE) force plus the short range quark exchange force based on the quark cluster model (QCM). We also include the Coulomb potential between the charged baryons. The parameters of the OBE, the cutoff parameters and the coupling constant of σ meson, are determined so that the NN data are reproduced in the same model. By fitting the deuteron binding energy and the S-wave scattering lengths, four parameter sets for the OBE and QCM are obtained.

We have applied these potentials to the two-body $\Lambda_c - N$ systems coupled with the $\Sigma_c - N$ and $\Sigma_c^* - N$ channels. The coupled-channel Schrödinger equations are solved to a good precision by the Gaussian expansion method. We find shallow bound states of $\Lambda_c N$ both in the $J^\pi = 0^+$ and 1^+ systems in two among the four parameter sets. Those parameters are the cases when the ranges of the QCM repulsion are small and thus the quark exchange effect is weaker than the other two. The difference between the $J^\pi = 0^+$ ($\Lambda_c N(^1S_0)$) and 1^+ ($\Lambda_c N(^3S_1)$) systems is small, which may be a consequence of the heavy quark spin symmetry. We note, however, that finite masses of Λ_c , Σ_c , and Σ_c^* occur heavy quark symmetry violation although the $1/M$ correction is very small. It is not surprising to have a bound state in these channels, because the $Y_c N$ interactions are similar to those of YN except for the K exchange part, while the kinetic energy is suppressed for the heavier baryon. Furthermore, the effect of the channel coupling to $\Sigma_c^* N$ is significant due to the strong tensor force coming from the one-pion exchange. We then conclude that shallow $\Lambda_c N$ bound states may exist.

Encouraged by the possible existence of the two-body bound states, we further consider three-body, $\Lambda_c NN$, bound states. This is the lightest “charmed nucleus”, which corresponds to the hyper-triton (Λpn) bound state in the strangeness sector. In order to simplify the calculation, in the present approach, we first construct an effective one-channel ($\Lambda_c N$) potential from the fully coupled ($\Lambda_c N - \Sigma_c N - \Sigma_c^* N$) calculation. Using the effective one-channel potential, we have solved three-body Schrödinger equation by the GEM and have obtained bound states with the binding energy about 20-22 MeV for $I = 0$, and 7-10 MeV for $I = 1$ from the $\Lambda_c NN$ threshold. The corresponding wave functions show that the Λ_c baryon makes the size of the NN system significantly smaller by attraction. In order to confirm these results, further studies with the full and explicit couplings of the $\Sigma_c N$ and Σ_c^* channels will be necessary.

Acknowledgment

S. M. is supported by the RIKEN Junior Research Associate Program. This work is supported in part by JSPS KAKENHI Grant Nos. 25247036, and 24250294. Y. R. L. was supported by the “Program for Promoting the Enhancement of Research Universities” at Tokyo Institute of Technology in 2014 and partly by NNSFC(No. 11275115).

References

- [1] D. Acosta et al. (CDF II Collaboration), Phys. Rev. Lett. **93**, 072001 (2004).
- [2] A. V. Manohar and M. B. Wise, Nucl. Phys. B **399** 17 (1993)
- [3] S. Ohkoda, Y. Yamaguchi, S. Yasui, K. Sudoh, and A. Hosaka, Phys. Rev. D **86**, 034019 (2012)
- [4] C.B. Dover and S.H. Kahana, Phys. Rev. Lett. **39**, 1506 (1977).
- [5] G. Bhamathi, Phys. Rev. C **24**, 181 (1981).
- [6] H. Bando and M. Bando, Phys. Lett. B **109**, 164 (1982); H. Bando and S. Nagata, Prog. Theor. Phys. **69**, 557 (1983); H. Bando, Prog. Theor. Phys. Suppl. **81**, 197 (1985).
- [7] B.F. Gibson, C.B. Dover, G. Bhamathi, and D.R. Lehman, Phys. Rev. C **27**, 2085 (1983).
- [8] Y.A. Batusov et al., JETP Lett. **33**, 56 (1981).
- [9] Y. R. Liu, and M. Oka, Phys. Rev. D **85**, 014015 (2012).
- [10] H. Garcilazo, A. Valcarce, and T.F. Carames, Phys. Rev. C **92** 024006 (2015).
- [11] M. Oka, and K. Yazaki, Phys. Lett. B **90**, 41 (1980); M. Oka, K. Shimizu, and K. Yazaki, Nucl. Phys. A **464** 700 (1987); M. Oka, K. Shimizu, and K. Yazaki, Prog. Theor. Phys. Suppl. **137** 1 (2000); M. Oka, Nucl. Phys. A, **881**, 6 (2012)
- [12] S. Takeuchi, O. Morimatsu, Y. Tani and M. Oka, Prog. Theor. Phys. Suppl. **137**, 83 (2000).
- [13] E. Hiyama, Y. Kino, and M. Kamimura, Prog. Part. Nucl. Phys. **51**, 223 (2003).
- [14] D. R. Thompson, M. Lemere, and Y. C. Tang, Nuci. Phys. A **286**, 53 (1977).
- [15] T. A. Rijken, M. M. Nagels and Y. Yamamoto, Prog. Theor. Phys. Suppl. **185**, 14 (2010).
- [16] R. B. Wiringa, V. G. J. Stoks and R. Schiavilla, Phys. Rev. C **51**, 38 (1995).
- [17] R. Machleidt, Phys. Rev. C **63**, 024001 (2001).
- [18] R. Tamagaki, Prog. Theor. Phys. **39**, 91 (1967).
- [19] N. Isgur and M.B. Wise, Phys. Lett. B **232**, 113 (1989).
- [20] M. Oka, Y. R. Liu, and W. Meguro, Few Body Syst. **54**, 1255 (2013).
- [21] S. Yasui, K. Sudoh, Y. Yamaguchi, S. Ohkoda, A. Hosaka, and T. Hyodo, Phys. Lett. B **727** 185 (2013).
- [22] Y. Yamaguchi, S. Ohkoda, A. Hosaka, T. Hyodo, and S. Yasui, Phys. Rev. D **91** 034034 (2015).
- [23] K. Nakamura et al. (Particle Data Group), J. Phys. G **37** 075021 (2010).
- [24] A. Manohar and H. Georgi, Nucl. Phys. B **234**, 189 (1984).
- [25] D. Jido, M. Oka, and A. Hosaka, Prog. Theor. Phys. **106**, 873 (2001).
- [26] S. Ishida et al., Prog. Thepr. Phys. **95**, 745 (1996).
- [27] K. Igi and K.I. Hisaka, Phys. Rev. D **59**, 034005 (1999).
- [28] G. Colangelo, J. Gasser, and H. Leutwyler, Nucl. Phys. B **603**, 125 (2001); I. Caprini, G. Colangelo, and H. Leutwyler, Phys. Rev. Lett. **96**, 132001 (2006).

Appendix A. Spin Matrix Elements of $Y_c N$ OBE potential

In this Appendix, definitions of the spin dependent operators in the potentials are given. \mathcal{O}_{spin} is the spin-spin operator between Y_c and N :

$$\mathcal{O}_{spin} = \mathcal{O}_1 \cdot \sigma_2, \quad (\text{A1})$$

where σ_2 is the Pauli matrix of the nucleon spin, and \mathcal{O}_1 is the spin operator of the charm baryon,

$$\mathcal{O}_1 = \begin{cases} \sigma_1 & \text{for } \Lambda_c \text{ and } \Sigma_c \\ \bar{\Sigma}_1 & \text{for the transition from } \Lambda_c \text{ and } \Sigma_c \text{ to } \Sigma_c^* N \\ \Sigma_1 & \text{for } \Sigma_c^* \end{cases} \quad (\text{A2})$$

The transition spin $\bar{\Sigma}$ is defined as $u^\mu \equiv \bar{\Sigma}\Phi$, where u^μ is the Rarita Schwinger field, and Φ is the spin wave functions of Σ_c^* ,

$$\Phi(3/2) = \begin{pmatrix} 1 \\ 0 \\ 0 \\ 0 \end{pmatrix}, \quad \Phi(1/2) = \begin{pmatrix} 0 \\ 1 \\ 0 \\ 0 \end{pmatrix}, \quad \Phi(-1/2) = \begin{pmatrix} 0 \\ 0 \\ 1 \\ 0 \end{pmatrix}, \quad \Phi(-3/2) = \begin{pmatrix} 0 \\ 0 \\ 0 \\ 1 \end{pmatrix}. \quad (\text{A3})$$

Then we calculate the transition spin explicit,

$$\begin{aligned} \bar{\Sigma}^\dagger &= -\frac{1}{\sqrt{2}} (\bar{\Sigma}_x^\dagger + i\bar{\Sigma}_y^\dagger) + \frac{1}{\sqrt{2}} (\bar{\Sigma}_x^\dagger - i\bar{\Sigma}_y^\dagger) + \bar{\Sigma}_z^\dagger \\ &= \begin{pmatrix} 1 & 0 & 0 & 0 \\ 0 & \sqrt{\frac{1}{3}} & 0 & 0 \end{pmatrix} + \begin{pmatrix} 0 & \sqrt{\frac{2}{3}} & 0 & 0 \\ 0 & 0 & \sqrt{\frac{2}{3}} & 0 \end{pmatrix} + \begin{pmatrix} 0 & 0 & \sqrt{\frac{1}{3}} & 0 \\ 0 & 0 & 0 & 1 \end{pmatrix} \end{aligned} \quad (\text{A4})$$

$$\bar{\Sigma}\bar{\Sigma}^\dagger = -I_{4 \times 4}, \quad \bar{\Sigma}^\dagger\bar{\Sigma} = -2I_{2 \times 2}. \quad (\text{A5})$$

With $\hat{e}(\lambda = +1) = -\frac{1}{\sqrt{2}}(1, i, 0)$, $\hat{e}(\lambda = -1) = \frac{1}{\sqrt{2}}(1, -i, 0)$, $\hat{e}(\lambda = 0) = (0, 0, 1)$, and $S_{t\mu}^\dagger = (0, \bar{S}_t^\dagger)$,

$$\bar{\Sigma}(1, +1) = \begin{pmatrix} 1 & 0 \\ 0 & \sqrt{\frac{1}{3}} \\ 0 & 0 \\ 0 & 0 \end{pmatrix}, \quad \bar{\Sigma}(1, -1) = \begin{pmatrix} 0 & 0 \\ 0 & 0 \\ \sqrt{\frac{1}{3}} & 0 \\ 0 & 1 \end{pmatrix}, \quad \bar{\Sigma}(1, 0) = \begin{pmatrix} 0 & 0 \\ \sqrt{\frac{2}{3}} & 0 \\ 0 & \sqrt{\frac{2}{3}} \\ 0 & 0 \end{pmatrix} \quad (\text{A6})$$

Next, we defined the spin operator of Σ_c^* , defined

$$\begin{aligned} \Sigma &= -S_{t\mu}^\dagger \sigma S_t^\mu = (S_t^\dagger)^j \sigma (S_t)^j, \\ \mathbf{S}(\Sigma_c^*) &= \frac{3}{2}\Sigma. \end{aligned} \quad (\text{A7})$$

With values in eq. (A6), we give the explicit values of matrices.

$$\begin{aligned}
\sigma_{rs}(1, +1) &= -\frac{1}{\sqrt{2}} (\Sigma_x + i\Sigma_y) = - \begin{pmatrix} 0 & \sqrt{\frac{2}{3}} & 0 & 0 \\ 0 & 0 & \frac{2\sqrt{2}}{3} & 0 \\ 0 & 0 & 0 & \sqrt{\frac{2}{3}} \\ 0 & 0 & 0 & 0 \end{pmatrix}, \\
\sigma_{rs}(1, -1) &= \frac{1}{\sqrt{2}} (\Sigma_x - i\Sigma_y) = - \begin{pmatrix} 0 & 0 & 0 & 0 \\ \sqrt{\frac{2}{3}} & 0 & 0 & 0 \\ 0 & \frac{2\sqrt{2}}{3} & 0 & 0 \\ 0 & 0 & \sqrt{\frac{2}{3}} & 0 \end{pmatrix}, \\
\sigma_{rs}(1, 0) &= \Sigma_z = - \begin{pmatrix} 1 & 0 & 0 & 0 \\ 0 & \frac{1}{3} & 0 & 0 \\ 0 & 0 & -\frac{1}{3} & 0 \\ 0 & 0 & 0 & -1 \end{pmatrix}.
\end{aligned} \tag{A8}$$

The tensor operators can be defined similarly as follows

$$\begin{aligned}
\text{In } \Lambda_c \text{ and } \Sigma_c \text{ channels} : \mathcal{O}_{\text{ten}} &= \frac{3(\sigma_1 \cdot \mathbf{r})(\sigma_2 \cdot \mathbf{r})}{r^2} - \sigma_1 \cdot \sigma_2, \\
\text{In } \Lambda_c \rightarrow \Sigma_c^* \text{ and } \Sigma_c \rightarrow \Sigma_c^* \text{ channels} : \mathcal{O}_{\text{ten}} &= \frac{3(\bar{\Sigma} \cdot \mathbf{r})(\sigma_2 \cdot \mathbf{r})}{r^2} - \bar{\Sigma} \cdot \sigma_2, \\
\text{In } \Sigma_c^* \text{ diagonal channels} : \mathcal{O}_{\text{ten}} &= \frac{3(\Sigma \cdot \mathbf{r})(\sigma_2 \cdot \mathbf{r})}{r^2} - \Sigma \cdot \sigma_2,
\end{aligned} \tag{A9}$$

The spin-orbit operator \mathcal{O}_{LS} is defined as

$$\mathcal{O}_{LS} = \mathbf{L} \cdot \sigma_2. \tag{A10}$$

$\mathbf{L} \cdot \mathcal{O}_1$ is not included in the potential for this calculation.

Appendix A.1. $I = \frac{1}{2}, J^\pi = 0^+$ coupled system

Tables A1-A3 give the matrix elements of \mathcal{O}_{spin} , \mathcal{O}_{ten} , \mathcal{O}_{ls} for the channels in $I = 1/2$, $J^\pi = 0^+$. We label the relevant channels by i and j , and tabulate the ij component of the matrix elements $\langle \mathcal{O} \rangle_{ij}$.

$\begin{array}{c} \diagdown \\ i \end{array} \quad \begin{array}{c} j \\ \diagup \end{array}$	$\Lambda_c N(^1S_0)$	$\Sigma_c N(^1S_0)$	$\Sigma_c^* N(^5D_0)$
$\Lambda_c N(^1S_0)$	-3	-3	0
$\Sigma_c N(^1S_0)$	-3	-3	0
$\Sigma_c^* N(^5D_0)$	0	0	1

Table A1 The matrix elements of the spin-spin operators $\langle \mathcal{O}_{spin} \rangle_{ij}$ for the $I = \frac{1}{2}, J^\pi = 0^+$ coupled system.

$\begin{array}{c} \diagdown \\ i \end{array} \quad \begin{array}{c} j \\ \diagup \end{array}$	$\Lambda_c N(^1S_0)$	$\Sigma_c N(^1S_0)$	$\Sigma_c^* N(^5D_0)$
$\Lambda_c N(^1S_0)$	0	0	$-\sqrt{6}$
$\Sigma_c N(^1S_0)$	0	0	$-\sqrt{6}$
$\Sigma_c^* N(^5D_0)$	$-\sqrt{6}$	$-\sqrt{6}$	-2

Table A2 The matrix elements of the tensor operators $\langle \mathcal{O}_{ten} \rangle_{ij}$ for the $I = \frac{1}{2}, J^\pi = 0^+$ coupled system.

$\begin{array}{c} \diagdown \\ i \end{array} \quad \begin{array}{c} j \\ \diagup \end{array}$	$\Lambda_c N(^1S_0)$	$\Sigma_c N(^1S_0)$	$\Sigma_c^* N(^5D_0)$
$\Lambda_c N(^1S_0)$	0	0	0
$\Sigma_c N(^1S_0)$	0	0	0
$\Sigma_c^* N(^5D_0)$	0	0	-3

Table A3 The matrix elements of the orbital-spin operators $\langle \mathcal{O}_{LS} \rangle_{ij}$ for the $I = \frac{1}{2}, J^\pi = 0^+$ coupled system.

Appendix A.2. $I = \frac{1}{2}$, $J^\pi = 1^+$ coupled system

For $I = 1/2$, $J^\pi = 1^+$, the matrix elements are given by Tables A4-A6.

$\begin{smallmatrix} & j \\ i & \end{smallmatrix}$	$\Lambda_c N(^3S_1)$	$\Sigma_c N(^3S_1)$	$\Sigma_c^* N(^3S_1)$	$\Lambda_c N(^3D_1)$	$\Sigma_c N(^3D_1)$	$\Sigma_c^* N(^3D_1)$	$\Sigma_c^* N(^5D_1)$
$\Lambda_c N(^3S_1)$	1	1	$-\sqrt{\frac{8}{3}}$	0	0	0	0
$\Sigma_c N(^3S_1)$	1	1	$-\sqrt{\frac{8}{3}}$	0	0	0	0
$\Sigma_c^* N(^3S_1)$	$-\sqrt{\frac{8}{3}}$	$-\sqrt{\frac{8}{3}}$	$-\frac{5}{3}$	0	0	0	0
$\Lambda_c N(^3D_1)$	0	0	0	1	1	$-\sqrt{\frac{8}{3}}$	0
$\Sigma_c N(^3D_1)$	0	0	0	1	1	$-\sqrt{\frac{8}{3}}$	0
$\Sigma_c^* N(^3D_1)$	0	0	0	$-\sqrt{\frac{8}{3}}$	$-\sqrt{\frac{8}{3}}$	$-\frac{5}{3}$	0
$\Sigma_c^* N(^5D_1)$	0	0	0	0	0	0	1

Table A4 The matrix elements of the spin-spin operators $\langle \mathcal{O}_{spin} \rangle_{ij}$ for the $I = \frac{1}{2}$, $J^\pi = 1^+$ coupled system.

$\begin{smallmatrix} & j \\ i & \end{smallmatrix}$	$\Lambda_c N(^3S_1)$	$\Sigma_c N(^3S_1)$	$\Sigma_c^* N(^3S_1)$	$\Lambda_c N(^3D_1)$	$\Sigma_c N(^3D_1)$	$\Sigma_c^* N(^3D_1)$	$\Sigma_c^* N(^5D_1)$
$\Lambda_c N(^3S_1)$	0	0	0	$\sqrt{8}$	$\sqrt{8}$	$\frac{1}{\sqrt{3}}$	$\sqrt{3}$
$\Sigma_c N(^3S_1)$	0	0	0	$\sqrt{8}$	$\sqrt{8}$	$\frac{1}{\sqrt{3}}$	$\sqrt{3}$
$\Sigma_c^* N(^3S_1)$	0	0	0	$\frac{1}{\sqrt{3}}$	$\frac{1}{\sqrt{3}}$	$-\frac{\sqrt{2}}{3}$	$-\sqrt{2}$
$\Lambda_c N(^3D_1)$	$\sqrt{8}$	$\sqrt{8}$	$\frac{1}{\sqrt{3}}$	-2	-2	$-\frac{1}{\sqrt{6}}$	$\sqrt{\frac{3}{2}}$
$\Sigma_c N(^3D_1)$	$\sqrt{8}$	$\sqrt{8}$	$\frac{1}{\sqrt{3}}$	-2	-2	$-\frac{1}{\sqrt{6}}$	$\sqrt{\frac{3}{2}}$
$\Sigma_c^* N(^3D_1)$	$\frac{1}{\sqrt{3}}$	$\frac{1}{\sqrt{3}}$	$-\frac{\sqrt{2}}{3}$	$-\frac{1}{\sqrt{6}}$	$-\frac{1}{\sqrt{6}}$	$\frac{1}{3}$	-1
$\Sigma_c^* N(^5D_1)$	$\sqrt{3}$	$\sqrt{3}$	$-\sqrt{2}$	$\sqrt{\frac{3}{2}}$	$\sqrt{\frac{3}{2}}$	-1	-1

Table A5 The matrix elements of the tensor operators $\langle \mathcal{O}_{ten} \rangle_{ij}$ for the $I = \frac{1}{2}$, $J^\pi = 1^+$ coupled system.

$\begin{smallmatrix} & j \\ i & \end{smallmatrix}$	$\Lambda_c N(^3S_1)$	$\Sigma_c N(^3S_1)$	$\Sigma_c^* N(^3S_1)$	$\Lambda_c N(^3D_1)$	$\Sigma_c N(^3D_1)$	$\Sigma_c^* N(^3D_1)$	$\Sigma_c^* N(^5D_1)$
$\Lambda_c N(^3S_1)$	0	0	0	0	0	0	0
$\Sigma_c N(^3S_1)$	0	0	0	0	0	0	0
$\Sigma_c^* N(^3S_1)$	0	0	0	0	0	0	0
$\Lambda_c N(^3D_1)$	0	0	0	-3	-3	0	0
$\Sigma_c N(^3D_1)$	0	0	0	-3	-3	0	0
$\Sigma_c^* N(^3D_1)$	0	0	0	0	0	$\frac{3}{2}$	$-\frac{3}{2}$
$\Sigma_c^* N(^5D_1)$	0	0	0	0	0	$-\frac{3}{2}$	$-\frac{3}{2}$

Table A6 The matrix elements of the orbital-spin operators $\langle \mathcal{O}_{LS} \rangle_{ij}$ for the $I = \frac{1}{2}$, $J^\pi = 1^+$ coupled system.

Appendix B. Definitions of the radial functions and coupling constants

Appendix B.1. The explicit forms of the radial functions

The Yukawa potential functions in eq. (1) are defined as

$$\begin{aligned}
Y(x) &= \frac{e^{-x}}{x}, \\
Z(x) &= \left(\frac{1}{x} + \frac{1}{x^2}\right)Y(x), \\
H(x) &= \left(1 + \frac{3}{x} + \frac{3}{x^2}\right)Y(x), \\
Y_1(m, \Lambda, r) &= Y(mr) - \left(\frac{\Lambda}{m}\right)Y(\Lambda r) - \frac{\Lambda^2 - m^2}{2m\Lambda}e^{-\Lambda r}, \\
Y_3(m, \Lambda, r) &= Y(mr) - \left(\frac{\Lambda}{m}\right)Y(\Lambda r) - \frac{(\Lambda^2 - m^2)\Lambda}{2m^3}e^{-\Lambda r}, \\
Z_3(m, \Lambda, r) &= Z(mr) - \left(\frac{\Lambda}{m}\right)^3 Z(\Lambda r) - \frac{(\Lambda^2 - m^2)\Lambda}{2m^3}Y(\Lambda r), \\
H_3(m, \Lambda, r) &= H(mr) - \left(\frac{\Lambda}{m}\right)^3 H(\Lambda r) - \frac{(\Lambda^2 - m^2)\Lambda}{2m^3}Y(\Lambda r) - \frac{(\Lambda^2 - m^2)\Lambda}{2m^3}e^{-\Lambda r}. \quad (\text{B1})
\end{aligned}$$

In eq. (B1), Λ is a cutoff parameter introduced for the monopole type form factor

$$F(q) = \frac{\Lambda^2 - m^2}{\Lambda^2 - q^2}, \quad (\text{B2})$$

where m is the mass of the exchanged meson and q is the 4-dimensional momentum of the meson. We use the following values of the meson masses: $m_\pi = 137.27[\text{MeV}]$, $m_\sigma = 600.0[\text{MeV}]$.

Appendix B.2. The coupling constants for the meson-exchange potentials

The coupling constants are given by Tables B1 and B2,

C_π	$\Lambda_c N$	$\Sigma_c N$	$\Sigma_c^* N$
$\Lambda_c N$	0	$(-\frac{\sqrt{6}}{2}g_2 g_A)$	$(-\frac{\sqrt{6}}{2}g_4 g_A)$
$\Sigma_c N$		$(-g_1 g_A)$	$(-g_3 g_A)$
$\Sigma_c^* N$			$(g_5 g_A)$

Table B1 C_π for the $Y_c N$ systems

C_σ	$\Lambda_c N$	$\Sigma_c N$	$\Sigma_c^* N$
$\Lambda_c N$	$(2l_B h_\sigma)$		
$\Sigma_c N$		$(-l_S h_\sigma)$	
$\Sigma_c^* N$			$(-l_S h_\sigma)$

Table B2 C_σ for the $Y_c N$ systems

with the following values [23–28]:

$$\begin{aligned}
g_2 &= -0.598, \quad g_4 = 0.999, \quad g_1 = \frac{\sqrt{8}}{3}g_4, \quad g_3 = \sqrt{\frac{2}{3}}g_4, \quad g_5 = -\sqrt{2}g_4, \\
g_A &= 1.25, \quad l_B = -3.1, \quad l_S = -2l_B,
\end{aligned}$$

and h_σ is a free parameter to be determined in sect. 2.4 The explicit values of the coupling constants are given as in Table B3 and B4

For the NN potential, we note that the function $Y_3(m, \Lambda, r)$ is used in place of $Y_1(m, \Lambda, r)$ in the π exchange potential and we use the coupling constants given in Tables B5 and B6.

C_π	$\Lambda_c N$	$\Sigma_c N$	$\Sigma_c^* N$
$\Lambda_c N$	0	0.92	-1.53
$\Sigma_c N$		-1.18	-1.02
$\Sigma_c^* N$			-1.77

Table B3 $Y_c N$ potential C_π values

C_σ	$\Lambda_c N$	$\Sigma_c N$	$\Sigma_c^* N$
$\Lambda_c N$	$(-6.2h_\sigma)$		
$\Sigma_c N$		$(-6.2h_\sigma)$	
$\Sigma_c^* N$			$(-6.2h_\sigma)$

Table B4 $Y_c N$ potential C_σ values

C_π	$NN(I=0)$	$NN(I=1)$
$NN(I=0)$	$\frac{1}{2}g_A^2$	
$NN(I=1)$		$\frac{3}{2}g_A^2$

Table B5 C_π for the NN systems

C_σ	$NN(I=0)$	$NN(I=1)$
$NN(I=0)$	$-h_\sigma^2$	
$NN(I=1)$		$-h_\sigma^2$

Table B6 C_σ for the NN systems

Appendix C. $Y_c N$ potentials

Here we give the figures of the $Y_c N$ potentials in the present calculation. The potentials for $J^\pi = 0^+$ are given in Figs. 3 - 8 in sect. 2.4.

Appendix C.1. Components of the $Y_c N$ CTNN-a potential ($J^\pi = 0^+$)

The individual contributions of one-pion exchange, one σ exchange, and QCM repulsion are given in Figs. C1 - C3 for $J^\pi = 0^+$ CTNN-a potential. One sees that one σ exchange is strongly attractive, so that even with the QCM repulsion the total potential becomes attractive. The similar behavior is seen for CTNN-b,c,d potentials.

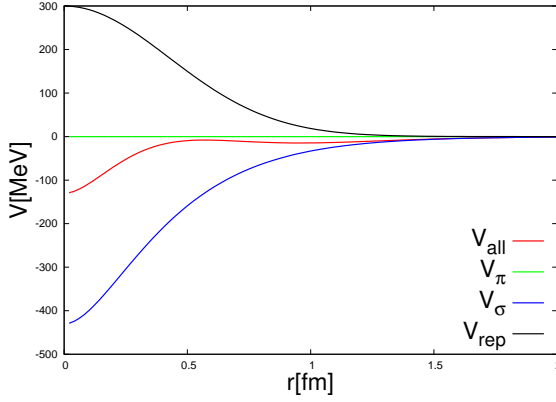


Fig. C1 $Y_c N$ -CTNN potential for $\Lambda_c N$ single channel

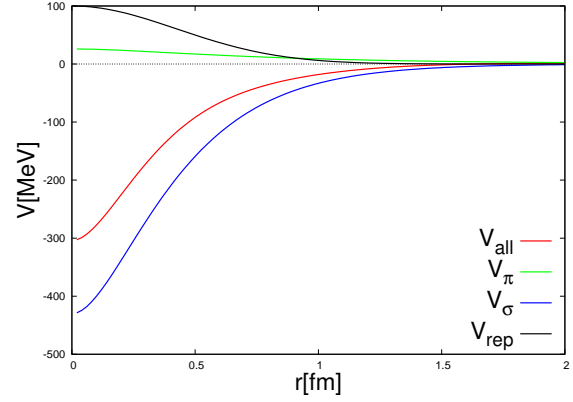


Fig. C2 $Y_c N$ -CTNN potential for $\Sigma_c N$ single channel

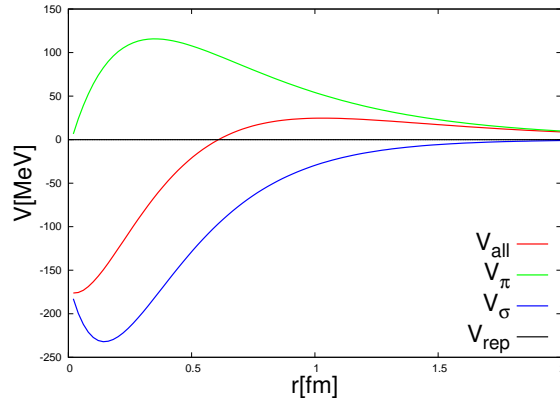


Fig. C3 $Y_c N$ -CTNN potential for $\Sigma_c^* N$ single channel

Appendix C.2. $Y_c N$ potentials ($J^\pi = 1^+$)

Figs. C4 - C29 show the $J^\pi = 1^+ Y_c N$ potentials. Four lines correspond to the four choices of the parameter sets, a ~ d. The potential for the diagonal $\Lambda_c N(^3S_1)$ channel is not shown here as it coincides with that for $\Lambda_c N(^1S_0)$. The off-diagonal potential $\Lambda_c N(^3S_1 - ^3D_1)$ is zero.

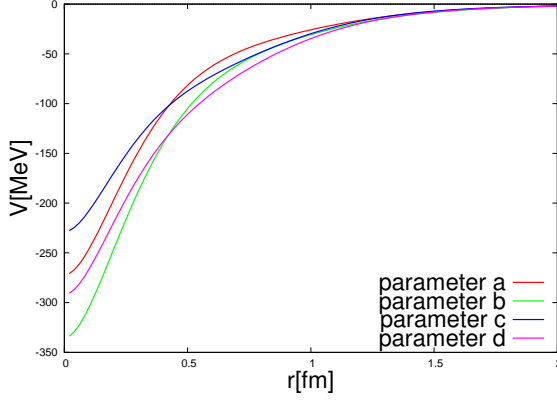


Fig. C4 $\Sigma_c N(^3S_1)$ diagonal potential.

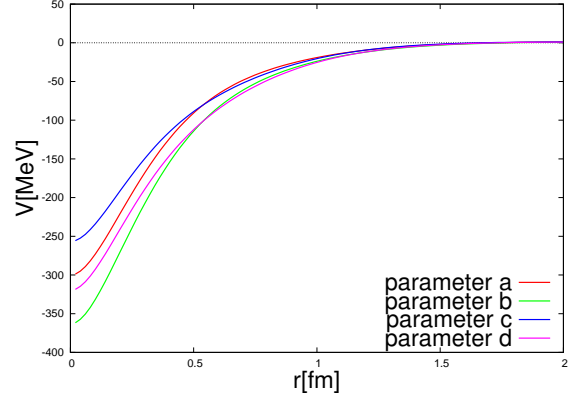


Fig. C5 $\Sigma_c^* N(^3S_1)$ diagonal potential.

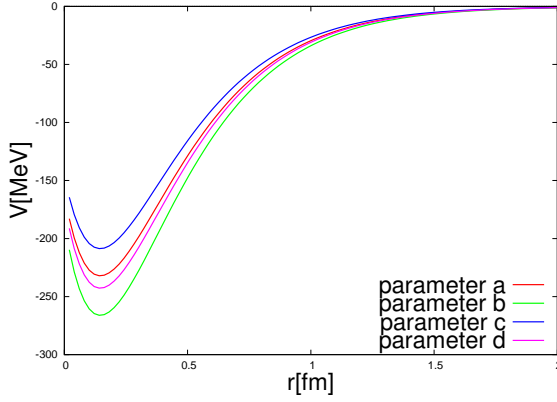


Fig. C6 $\Lambda_c N(^3D_1)$ diagonal potential.

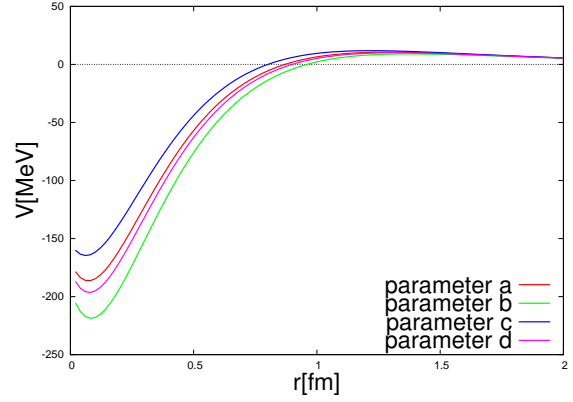


Fig. C7 $\Sigma_c N(^3D_1)$ diagonal potential.

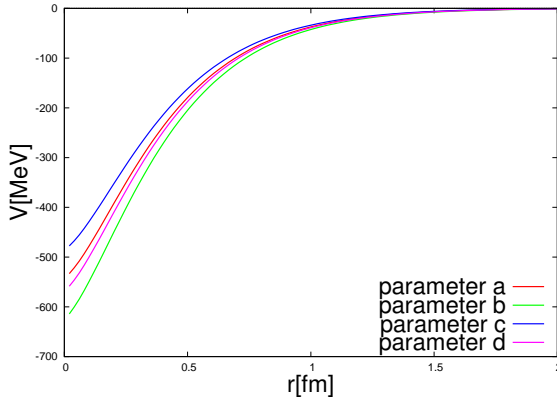


Fig. C8 $\Sigma_c^* N(^3D_1)$ diagonal potential.

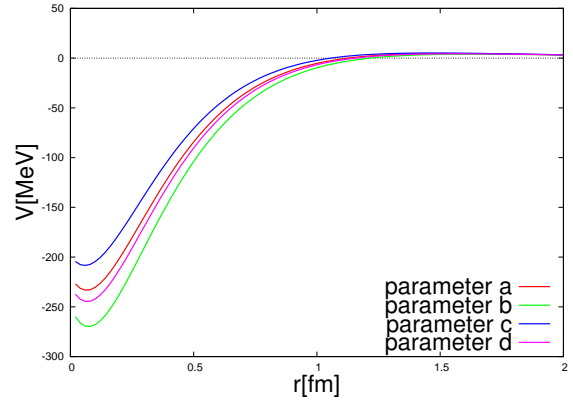


Fig. C9 $\Sigma_c^* N(^5D_1)$ diagonal potential.

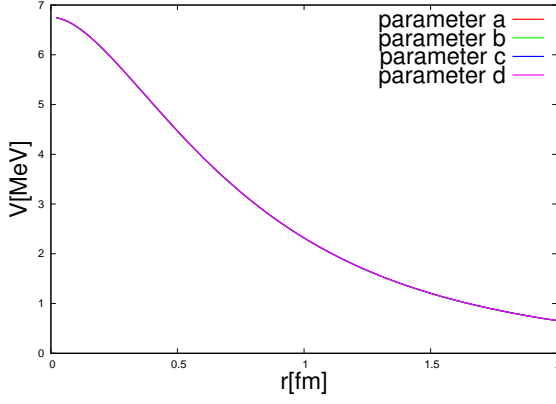


Fig. C10 $\Lambda_c N(^3S_1) - \Sigma_c N(^3S_1)$.

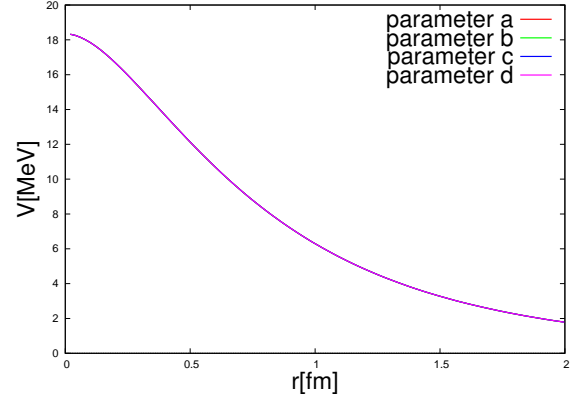


Fig. C11 $\Lambda_c N(^3S_1) - \Sigma_c^* N(^3S_1)$.

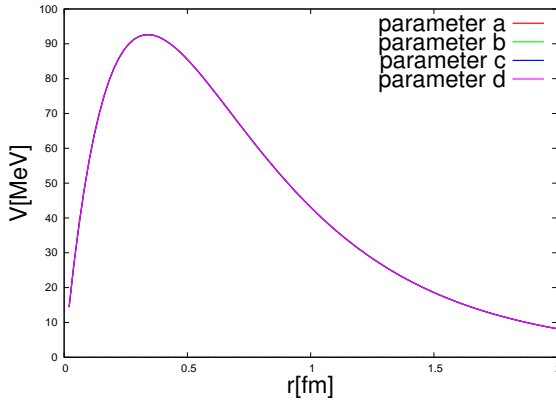


Fig. C12 $\Lambda_c N(^3S_1) - \Sigma_c N(^3D_1)$.

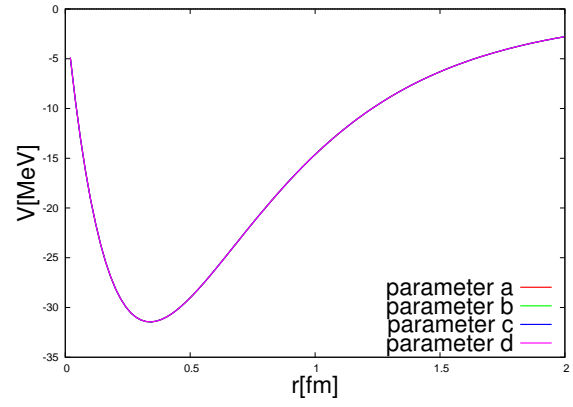


Fig. C13 $\Lambda_c N(^3S_1) - \Sigma_c^* N(^3D_1)$.

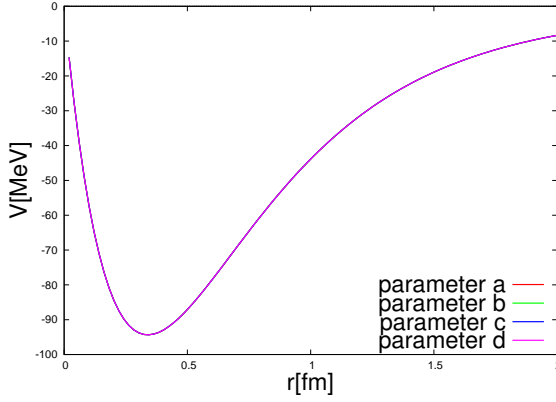


Fig. C14 $\Lambda_c N(^3S_1) - \Sigma_c^* N(^3D_1)$.

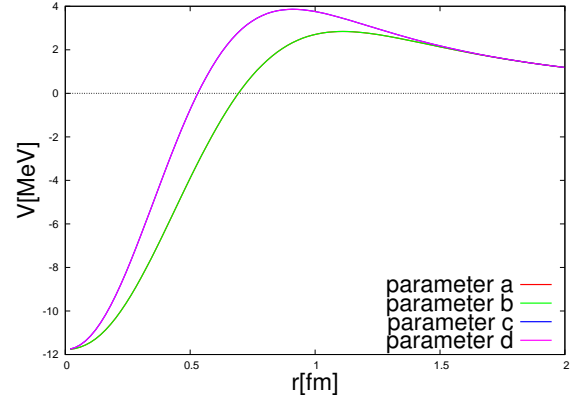


Fig. C15 $\Sigma_c N(^3S_1) - \Sigma_c^* N(^3S_1)$.

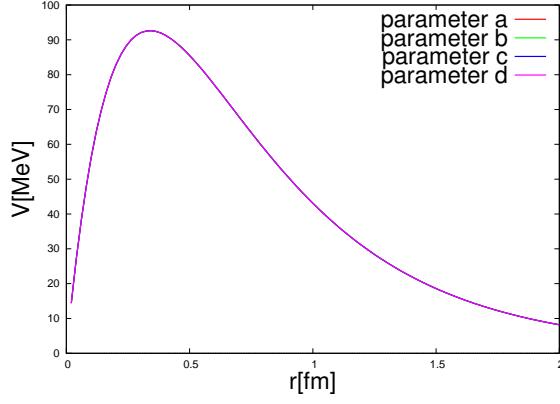


Fig. C16 $\Sigma_c N(^3S_1) - \Lambda_c N(^3D_1)$.

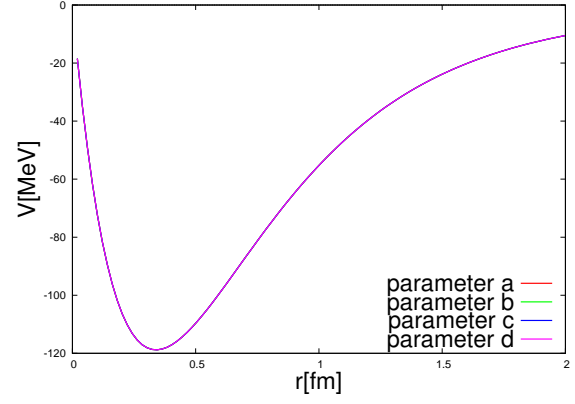


Fig. C17 $\Sigma_c N(^3S_1) - \Sigma_c N(^3D_1)$.

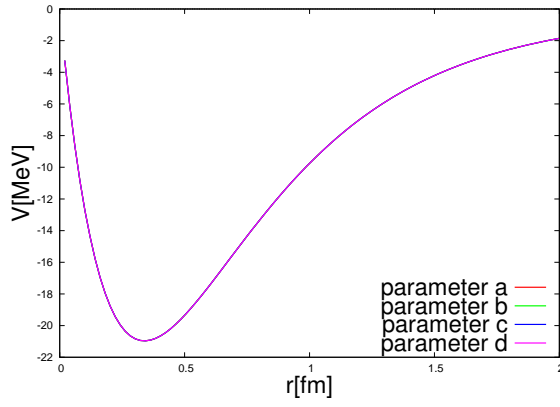


Fig. C18 $\Sigma_c N(^3S_1) - \Sigma_c^* N(^3D_1)$.

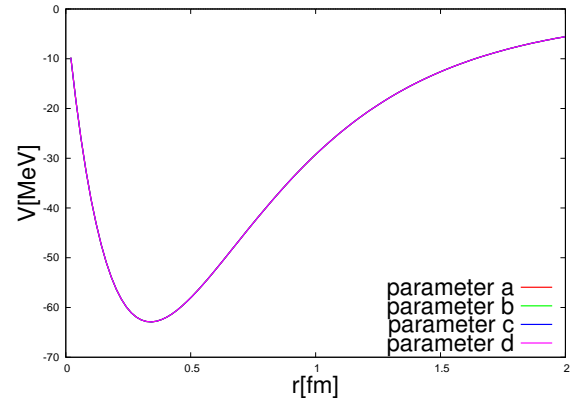


Fig. C19 $\Sigma_c N(^3S_1) - \Sigma_c^* N(^5D_1)$.

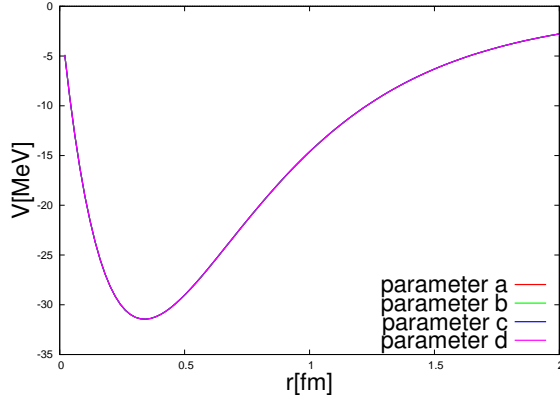


Fig. C20 $\Sigma_c^* N(^3S_1) - \Lambda_c N(^3D_1)$.

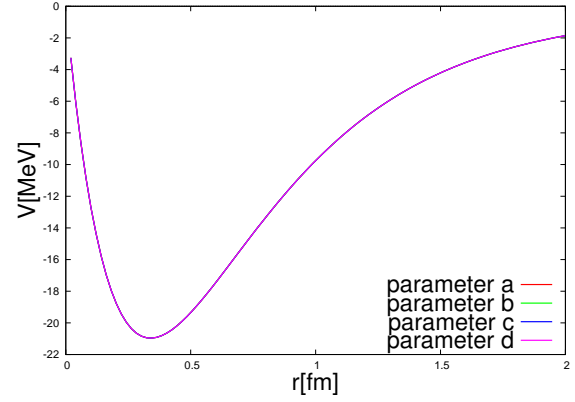


Fig. C21 $\Sigma_c^* N(^3S_1) - \Sigma_c N(^3D_1)$.

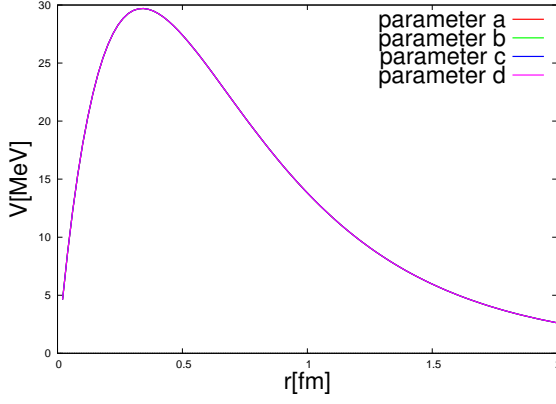


Fig. C22 $\Sigma_c^* N(^3S_1) - \Sigma_c^* N(^3D_1)$.

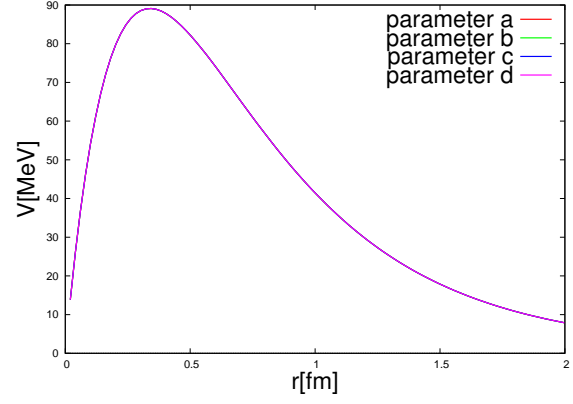


Fig. C23 $\Sigma_c^* N(^3S_1) - \Sigma_c^* N(^5D_1)$.

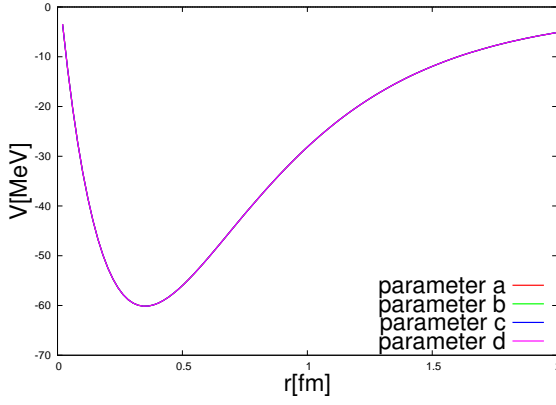


Fig. C24 $\Lambda_c N(^3D_1) - \Sigma_c N(^3D_1)$.

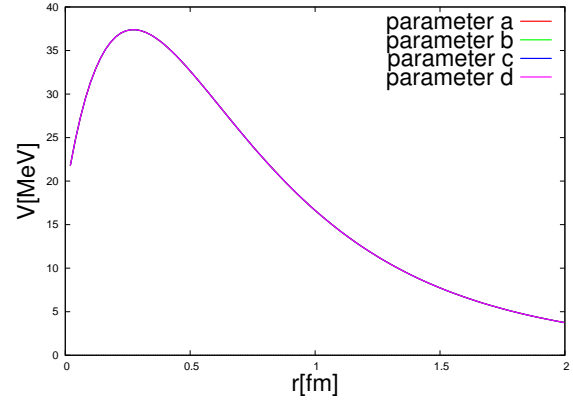


Fig. C25 $\Lambda_c N(^3D_1) - \Sigma_c^* N(^3D_1)$.

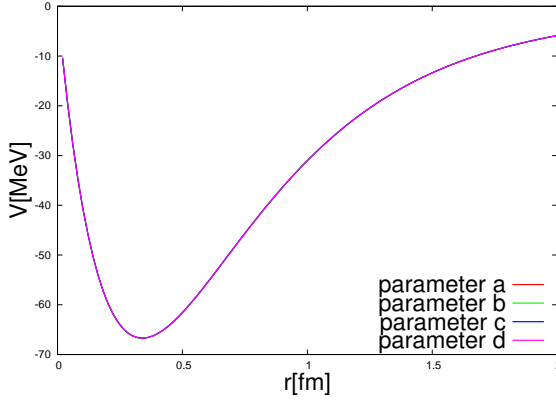


Fig. C26 $\Lambda_c N(^3D_1) - \Sigma_c^* N(^5D_1)$.

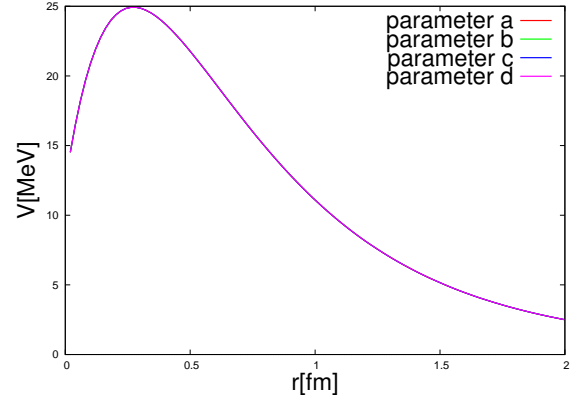


Fig. C27 $\Sigma_c N(^3D_1) - \Sigma_c^* N(^3D_1)$.

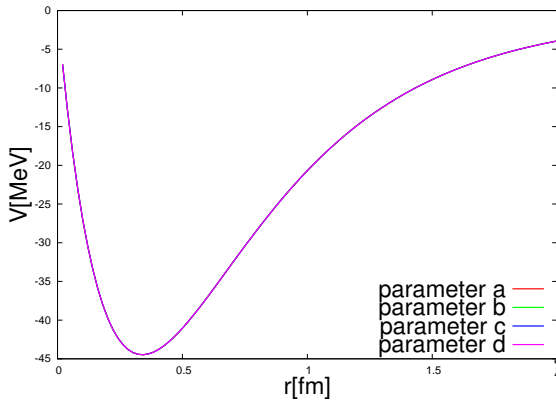


Fig. C28 $\Sigma_c N(^3D_1) - \Sigma_c^* N(^5D_1)$.

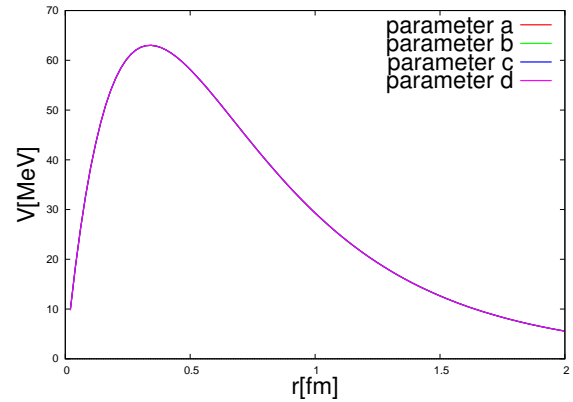


Fig. C29 $\Sigma_c^* N(^3D_1) - \Sigma_c^* N(^5D_1)$.

